Am J Physiol Cell Physiol 307: C910–C919, 2014.
First published August 27, 2014; doi:10.1152/ajpcell.00192.2013.

Diabetes increases stiffness of live cardiomyocytes measured by atomic force microscopy nanoindentation

Juan C. Benech,[1] Nicolás Benech,[2] Ana I. Zambrana,[1] Inés Rauschert,[1] Verónica Bervejillo,[1] Natalia Oddone,[1] and Juan P. Damián[1,3]

[1]*Laboratorio de Señalización Celular y Nanobiología, Instituto de Investigaciones Biológicas Clemente Estable, Montevideo, Uruguay;* [2]*Instituto de Física, Facultad de Ciencias, Universidad de la República, Montevideo, Uruguay; and* [3]*Departamento de Biología Molecular y Celular, Facultad de Veterinaria, Universidad de la República, Montevideo, Uruguay*

Submitted 24 June 2013; accepted in final form 4 August 2014

Benech JC, Benech N, Zambrana AI, Rauschert I, Bervejillo V, Oddone N, Damián JP. Diabetes increases stiffness of live cardiomyocytes measured by atomic force microscopy nanoindentation. *Am J Physiol Cell Physiol* 307: C910–C919, 2014. First published August 27, 2014; doi:10.1152/ajpcell.00192.2013.—Stiffness of live cardiomyocytes isolated from control and diabetic mice was measured using the atomic force microscopy nanoindentation method. Type 1 diabetes was induced in mice by streptozotocin administration. Histological images of myocardium from mice that were diabetic for 3 mo showed disorderly lineup of myocardial cells, irregularly sized cell nuclei, and fragmented and disordered myocardial fibers with interstitial collagen accumulation. Phalloidin-stained cardiomyocytes isolated from diabetic mice showed altered (i.e., more irregular and diffuse) actin filament organization compared with cardiomyocytes from control mice. Sarco/endoplasmic reticulum Ca^{2+}-ATPase (SERCA2a) pump expression was reduced in homogenates obtained from the left ventricle of diabetic animals compared with age-matched controls. The apparent elastic modulus (AEM) for live control or diabetic isolated cardiomyocytes was measured using the atomic force microscopy nanoindentation method in Tyrode buffer solution containing 1.8 mM Ca^{2+} and 5.4 mM KCl (physiological condition), 100 nM Ca^{2+} and 5.4 mM KCl (low extracellular Ca^{2+} condition), or 1.8 mM Ca^{2+} and 140 mM KCl (contraction condition). In the physiological condition, the mean AEM was 112% higher for live diabetic than control isolated cardiomyocytes (91 ± 14 vs. 43 ± 7 kPa). The AEM was also significantly higher in diabetic than control cardiomyocytes in the low extracellular Ca^{2+} and contraction conditions. These findings suggest that the material properties of live cardiomyocytes were affected by diabetes, resulting in stiffer cells, which very likely contribute to high diastolic LV stiffness, which has been observed in vivo in some diabetes mellitus patients.

atomic force microscopy; diabetes; live cardiomyocyte stiffness

THE PREVALENCE OF DIABETES mellitus is rapidly growing. It is estimated that, globally, the number of adults with diabetes mellitus will increase from 171 million in 2000 to 300 million by 2030 (35). Diabetes mellitus is a well-recognized risk factor for development of heart failure (HF). Indeed, the Framingham Heart Study showed that HF occurs twice as frequently in diabetic men and five times as frequently in diabetic women as in age-matched controls (12). Thus cardiovascular complications, such as increased atherosclerosis in large arteries (carotid artery, aorta, and femoral artery) and increased coronary atherosclerosis, which increases the risk for myocardial infarction and stroke, are the leading cause of diabetes-related morbidity and mortality (5, 11).

In animal models of diabetes, several cardiac functional and structural alterations or cardiac muscle disorders have been documented in type 1 and type 2 diabetes (5). In most of the type 1 diabetes studies, diabetes was induced by streptozotocin (STZ) administration (5, 24, 31). In humans, diabetes mellitus-induced diastolic left ventricular (LV) dysfunction is increasingly recognized as an important morbidity and mortality determinant in HF. In patients with diabetes mellitus, an increase in diastolic LV stiffness obstructs LV remodeling after myocardial infarction (27, 28) and raises LV filling pressures at similar LV filling volumes in HF with reduced LV ejection fraction and in HF with normal LV ejection fraction (32). As a consequence, diabetes mellitus patients have a higher incidence of HF after myocardial infarction (18, 23, 27, 28). Mechanisms that have been proposed to be responsible for raising myocardial stiffness in diabetes mellitus consist basically of excessive fibrosis (33) and deposition of advanced glycation end products (3). Hypertrophic cardiomyocytes isolated from LV biopsy samples of HF patients with normal LV ejection fraction showed high resting tension, which correlated with greater in vivo diastolic LV stiffness. This high resting tension might be an important contributor to the increased diastolic LV stiffness in the diabetic heart (32). Resting tension was measured in single cardiomyocytes isolated from frozen biopsy samples that were thawed, mechanically disrupted, and incubated with Triton X-100, provoking sarcolemmal and sarcoplasmic membrane disruption (4, 10, 32).

Atomic force microscopy (AFM) allows study of the dynamics and mechanical properties of intact cells. Different cell events, such as locomotion, differentiation and aging, physiological activation, electromotility, and cell pathology, can be analyzed with this new research tool (8, 13, 15, 17, 21, 37, 38). The effects of aging and obesity on vascular smooth muscle cell stiffness (8, 21, 38) and aging on cardiomyocyte stiffness (15) have been analyzed using AFM. However, to our knowledge, no studies have examined directly the effect of diabetes on the material properties of single live cardiomyocytes.

The present study, to the best of our knowledge, is the first to use the nanoindentation method of AFM to compare the material properties of live isolated LV myocytes from normal and diabetic mice.[1]

Address for reprint requests and other correspondence: J. C. Benech, Laboratorio de Señalización Celular y Nanobiología, Instituto de Investigaciones Biológicas Clemente Estable, Av. Italia 3318, CP 11600, Montevideo, Uruguay (e-mail: jbenech@iibce.edu.uy or juanclaudio.benech@gmail.com).

[1] This article is the topic of an Editorial Focus by Gerald A. Meininger (16a).

MATERIALS AND METHODS

Ethical approval. The experimental procedures were approved by the Institutional Ethical Committee (CEUA-IIBCE, Uruguay) in accordance with national legislation.

Experimental animals. STZ (Sigma, St. Louis, MO), which causes selective necrosis of pancreatic cells and results in an insulin deficiency state, was used to induce type 1 diabetes. Adult (1.5-mo-old) male CD1 mice ($n = 12$) were injected with a single dose (150 mg/kg ip) of a freshly prepared STZ solution in a citrate-saline buffer (pH 4.5). This dose of STZ was previously shown to result in high blood glucose levels with minimal cardiotoxicity (36). Control animals ($n = 12$) were injected with citrate buffer. Prior to STZ injection, all mice were weighed, and blood was obtained from the tail vein for measurement of nonfasting blood glucose using the ACCU-CHEK Compact Plus System (Indianapolis, IN). After 4–7 days of STZ administration, blood glucose was measured again, and mice with blood glucose >250 mg/dl were considered diabetic. For 3 mo, nonfasting blood glucose was monitored weekly to ensure continued diabetic status, as recommended by the manufacturer's instruction.

Variation in the apparent elastic modulus (AEM) was studied in 4.5-mo-old male control and diabetic CD1 mice. Diabetic mice were euthanized after 3 mo of diabetes. To obtain enough control and diabetic mice for the present study, this protocol was repeated once.

Statistical methods for animals. Body weight and glycemia were compared using ANOVA for repeated measurements. The model considered the group (diabetics vs. controls), time (in weeks), and interaction between group and time as fixed effects and the mouse in each group as a random effect. Post hoc comparisons were performed using least significant difference.

Morphological study. Hearts were rapidly removed from the mice and washed with phosphate-buffered saline (PBS) solution. Cardiac tissues were fixed in 3% paraformaldehyde for 1 h and cryoprotected in 15% and 30% sucrose, respectively (48 h). Thereafter they were embedded in tissue-freezing medium (Jung), sectioned, and stained with hematoxylin and eosin for light-microscopic morphological study.

F-actin study and confocal microscopy. Isolated cardiomyocytes from control and diabetic mice were fixed on polylysine-treated glass with 1% paraformaldehyde and later washed with 0.1% Triton X-100-PBS. Thereafter they were stained with 50 μg/ml fluorescent phalloidin 633 conjugate solution in PBS for 40 min at room temperature (Sigma-Aldrich). Finally, they were washed three times with PBS. Mounted samples were analyzed using confocal microscopy. A surface plot of selected cells was made using National Institutes of Health ImageJ software.

Preparation of protein lysate. For Western blot analysis, frozen heart tissue (50 mg) was homogenized in 1.5 ml of lysis buffer [20 mM HEPES (pH 7.4), 2 mM EGTA, 1 mM dithiothreitol, 1 mM sodium orthovanadate, 1% Triton X-100, 10% glycerol, 2 μM leupeptin, 1 mM aprotinin, and 400 μM phenylmethylsulfonylfluoride]. The homogenate was centrifuged at 4°C at 14,000 *g*, the supernatant was collected and sonicated, and the protein concentration was determined by Bradford assay. Tissue lysate aliquots were stored at −80°C.

Western blot analysis. Proteins (50 mg) were resolved by 10% SDS-PAGE and transferred to a polyvinylidene difluoride membrane, as previously described (1). Membranes were blocked with 10% fat-free milk and incubated overnight at 4°C with anti-sarco/endoplasmic reticulum Ca^{2+}-ATPase (SERCA2a, 1:500 dilution; product no. ab2861, Abcam) or anti-β-actin (1:1,000 dilution; product no. ab8227, Abcam) antibody. β-Actin was used as the loading control. Membranes were washed with 1× Tris-buffered saline (TBS)-Tween and hybridized with the appropriate secondary antibody conjugated with Alexa 488 in 1× TBS-Tween: Invitrogen A11001 (1:1,000 dilution) for SERCA2a and Invitrogen A11008 (1:5,000 dilution) for β-actin. After the membranes were washed, the signal was developed using a high-performance luminescent image analyzer (model FLA-9000, Fujifilm) according to the manufacturer's instructions. Protein bands were analyzed using ImageJ software.

Preparation of LV myocytes. Cardiomyocytes were prepared from control and diabetic male CD1 mice as described by Brum et al. (6) with modifications. The heart was rapidly excised and immediately immersed in a Tyrode buffer solution (TyBS; in mM: 135 NaCl, 5.4 KCl, 1.8 $CaCl_2$, 1 $MgCl_2$, 10 glucose, and 5 HEPES, pH 7.4). The excised heart was washed in TyBS to remove blood and immersed in Ca^{2+}-free TyBS (135 mM NaCl, 5.4 mM KCl, 50 μM EGTA, 1 mM $MgCl_2$, 10 mM glucose, and 5 mM HEPES, pH 7.4) for 10 min. A section of LV (30–40 mg) was cut into small pieces and incubated for 5 min in TyBS with 30 mg/ml collagenase type I and 50 μM Ca^{2+} (to enhance collagenase activity). Subsequently, the pieces of tissue were transferred to an Eppendorf flask containing TyBS with 50 μM Ca^{2+} and shaken to obtain single cells. The remaining pieces of tissue were removed from the flask, and the solution containing the cells was centrifuged for 5 min at 800 *g*. The pellet was resuspended in TyBS with 0.5 mM Ca^{2+} and centrifuged again for 5 min. This process was repeated in TyBS containing 1 mM Ca^{2+} and, finally, 1.8 mM Ca^{2+}. All solutions were warmed at 37°C and oxygenated. Myocytes were studied within 6 h from the time of isolation, as previously reported (15, 37). While cells were not analyzed with the AFM, they were kept in a CO_2-water-jacketed incubator (SANYO) in TyBS with 200 μM Ca^{2+}, which provided a 37°C, 5% CO_2-humidified environment. To quantify cardiomyocyte viability, cardiomyocytes were stained with propidium iodide (PI) in a petri dish chamber. Cells in the chamber were photographed using an Olympus IX81 inverted microscope. Total cells, as well as PI-stained (nonviable) cells, were counted. Control myocyte isolations yielded ~70% viable cells, whereas isolations in diabetic mice yielded ~60% viable cells.

AFM. AFM indentation tests were conducted with an atomic force microscope (BioScope Catalyst, Bruker). After isolation, myocytes in TyBS (1.8 mM or 200 μM Ca^{2+}) were plated on polylysine-coated glass microslide chambers (Sigma) for 10 min. Attached cardiomyocytes were incubated with PI for 5 min in darkness and washed carefully three times with TyBS with different ionic compositions: *1*) normal physiological condition, *2*) low extracellular Ca^{2+} condition, or *3*) contraction condition (see *Composition of TyBS*).

The plated myocytes were placed into the inverted Nikon microscope coupled to the AFM. Isolated cells were studied using an AFM fluid cantilever holder at 25°C. The absence of PI fluorescence was used for selection of viable isolated cardiomyocytes, and only these were measured. All AFM measurements were conducted within 1 h after insertion of the AFM head. The silicon nitride probe (DNP-10, Bruker; *cantilever D*), with a tip radius of 20–60 nm, was attached to a triangular 200-μm-long cantilever with a spring constant of 0.06 N/m, according to the manufacturer's instructions. The indentation protocol was as follows: *1*) a ×20 and ×40 magnification eyepiece was used to position the cantilever directly above the surface of an immobilized myocyte; *2*) a fast low-resolution 200- to 500-nm image of the middle of the longitudinal axis of the cardiomyocytes was obtained in the contact mode with the DNP-10 probe; and *3*) the "point-and-shoot" application of the AFM software was used to select a series of points over the obtained image. Proper force curves with an indentation-and-retraction rate of 6 μm/s were obtained in the force calibration mode at selected points. A low (1-Hz) frequency was set; this frequency was found to minimize not only hysteresis, but also drag force, and to maximize the number of force curves that were captured, as previously described (7, 14, 16, 22). At least 128 force curves were captured for each cell.

The indentation force (F) was calculated using Hooke's law, $F = k\delta$, where k is the cantilever's spring constant and δ is the cantilever's measured deflection. The spring constant k was calibrated using the thermal noise method ("thermal tune" application of Bruker AFM software) and was 0.067 N/m. The indentation depth h was calculated from the difference between the z movement of the piezoelectric

motor and the deflection (δ) of the cantilever. The equation relating the total elastic force exerted by the indenter (F_e) with pyramidal geometry over the sample is given by (26)

$$F_e = \frac{4E^* \tan(\alpha)}{\pi\sqrt{\pi}} h^2 \quad (1)$$

where E^* is the indenter sample's reduced Young's modulus, or AEM, and α is the half-pyramid angle. For indenters of a material much stiffer than the sample, the reduced Young's modulus is given approximately by $E^* \approx E/(1 - \nu^2)$, where E is Young's modulus and ν is the sample's Poisson ratio ($\nu \approx 0.5$ for incompressible materials such as the cell cytoplasm). *Equation 1* was used to fit the approaching curve from which E is retrieved. It is known from a previous report (26) that if the adhesive force at the tip-sample contact area is not negligible, the total force applied to the indenter during the unloading process is the sum of the elastic force given in *Eq. 1* and the adhesive force (F_a) at the indenter-sample contact area. The total force [$F(h)$] as a function of the indentation depth is given by

$$F(h) = \frac{4E \tan(\alpha)}{(1 - \nu\text{^}2)\pi\sqrt{\pi}} h^2 - \frac{32\gamma_\alpha}{\pi^2} \frac{\tan(\alpha)}{\cos(\alpha)} h \quad (2)$$

Thus the total force is composed of two terms. The first term is quadratic in h and accounts for the elastic force. The second term is linear in h and accounts for the adhesive force. This last term gives negative values of F at low values of h, a feature observed experimentally in unloading force curves obtained with AFM. *Equation 2* was used to fit the retracting curves and extract the work of adhesive forces (γ_a) from the linear term in h. We prefer to account for the effect of adhesion force by fitting all points for each retraction curve (*Eq. 2*), instead of determining the unbinding force (i.e., the rupture point in the retraction curve). This last method uses a single point of the curve and is affected by random noise fluctuations, resulting in higher dispersion.

Note that E can also be retrieved from the quadratic term of the retracting curve. However, this is not the usual practice, since the viscoelastic cell behavior introduces a hysteresis loop even at low rates. Thus the elasticity estimation differs between the approaching and the retracting curves.

Composition of TyBS solutions. For the normal physiological condition, TyBS with 1.8 mM Ca^{2+} (in mM: 135 NaCl, 5.4 KCl, 1.8 $CaCl_2$, 1 $MgCl_2$, 10 glucose, and 5 HEPES, pH 7.4) was used. For the low extracellular Ca^{2+} condition, TyBS with 100 nM free Ca^{2+} was used. The free Ca^{2+} concentration was calculated using the apparent Ca-EGTA association constants provided by Schwartzenbach and a computer program described by Fabiato and Fabiato (2, 9). The composition of the TyBS with 100 nM free Ca^{2+} was 135 mM NaCl, 5.4 mM KCl, 50 μM EGTA, 1 mM $MgCl_2$, 35.7 μM $CaCl_2$, 10 mM glucose, and 5 mM HEPES, pH 7.4. For the contraction condition, cells were incubated in high-K^+ TyBS (in mM: 5.4 NaCl, 140 KCl, 1.8 $CaCl_2$, 1 $MgCl_2$, 10 glucose, and 5 mM HEPES, pH 7.4).

AFM images. AFM images from fixed isolated cardiomyocytes were obtained with an atomic force microscope (BioScope Catalyst, Bruker). After isolation, cardiomyocytes were fixed for 10 min at 4°C in 3% paraformaldehyde, washed three times with MilliQ ultrapure water, and imaged using a silicon nitride probe (ScanAsyst-Air, Bruker). The probe had a tip radius of 2 nm, was attached to a triangular 115-μm-long cantilever, and had a spring constant of 0.4 N/m, according to the manufacturer's specifications. The images were obtained in the peak force tapping mode using the ScanAsyst-Air application (40 × 40-μm scan size and 640 × 640-pixel resolution) and were used to measure height of isolated cardiomyocytes.

Statistical methods for data analysis. A set of ~20 points from each cell image was selected using the point-and-shoot option of the AFM device. A minimum of 12 force curves were acquired for each point. From the data set for each cell type (control and diabetic), the force curves were fitted with a second-order polynomial. Since the ramp size of the force curve was kept constant during all measurements for each cell, some force curves were not properly acquired. Thus the fits with a correlation coefficient (r^2) <0.98 were discarded. Using *Eq.* 2, Young's modulus and the work of the adhesion force were retrieved. A normalized histogram for Young's modulus was constructed and fitted with a Gaussian curve. Data points outside the 95% confidence interval ($\bar{E} \pm 2\sigma$) were discarded, and the histogram and Gaussian fit were recalculated without these points. Then Student's *t*-test was used to determine if the two sets of data (control and diabetic) were significantly different from each other. This protocol was performed for all the experimental conditions.

All data are expressed as means ± SD. Student's *t*-test was used for comparison between groups. In all cases, $P < 0.05$ was considered significant.

RESULTS

Characterization of diabetic animals. In adult male mice, a single injection of STZ (150 mg/kg ip) resulted in high blood glucose levels (>250 mg/dl). In the 1st wk, there was no difference in body weight or glycemia level between the diabetic and control mice (Fig. 1, *A* and *B*). After the 2nd wk, body weight was lower ($P < 0.05$) and glycemia level was higher ($P < 0.0001$) in the diabetic than control mice. Blood glucose levels remained in the range of 160 mg/dl in vehicle-injected control animals and in animals prior to STZ injection (Fig. 1*A*). Over time, STZ-injected hyperglycemic animals developed symptoms of severe diabetes, characterized by polyuria, polydipsia, and poor body weight gain (Fig. 1, *B* and *D*). Figure 1*C* shows that 75% of these diabetic mice died before the end of the study (12–13 wk), while 91.6% of the animals in the control group survived.

Myocardial collagen accumulation, fragmentation of myocardial fibers, and inhibition of the SERCA2a pump. Hematoxylin-eosin-stained histological images showed well-arranged myocardial cells, with clear cellular nucleus and uniformly stained cytoplasm in the control group (Fig. 2, *A* and *B*). However, in diabetic animals, myocardial cells lined up in disorder, cellular nucleus sizes were irregular, and the myocardial fibers were fragmented and disordered. Moreover, the heart tissue contractile apparatus appeared severely disrupted (Fig. 2, *C* and *D*).

As previously shown (30), we detected interstitial collagen accumulation in heart tissue sections from diabetic mice (Fig. 2, *C* and *D*) compared with control mice (Fig. 2, *A* and *B*), where no collagen aggregates were observed. On the other hand, and consistent with previous reports (29–31), in LV homogenates from diabetic animals, we detected a reduction of SERCA2a pump expression compared with age-matched controls (Fig. 3). β-Actin was used as the loading control.

Viability of isolated cardiomyocytes and AFM images. Cardiomyocytes were isolated from control or diabetic mice and incubated with PI (see MATERIALS AND METHODS). Figure 4*B* shows a typical fluorescence image of myocytes isolated from control animals and incubated with PI. Figure 4*A* shows the normal-light image of the same preparation of isolated myocytes. Figure 4*C* depicts an isolated cardiomyocyte with the triangular AFM cantilever. Myocytes isolated from control animals were ~10% more viable (Ca^{2+}-resistant) than those from diabetic animals. AFM images from fixed isolated cardiomyocytes showed that the height of the smallest control cardiomyocytes was 2.5 ± 1.4 μm ($n = 40$) compared with

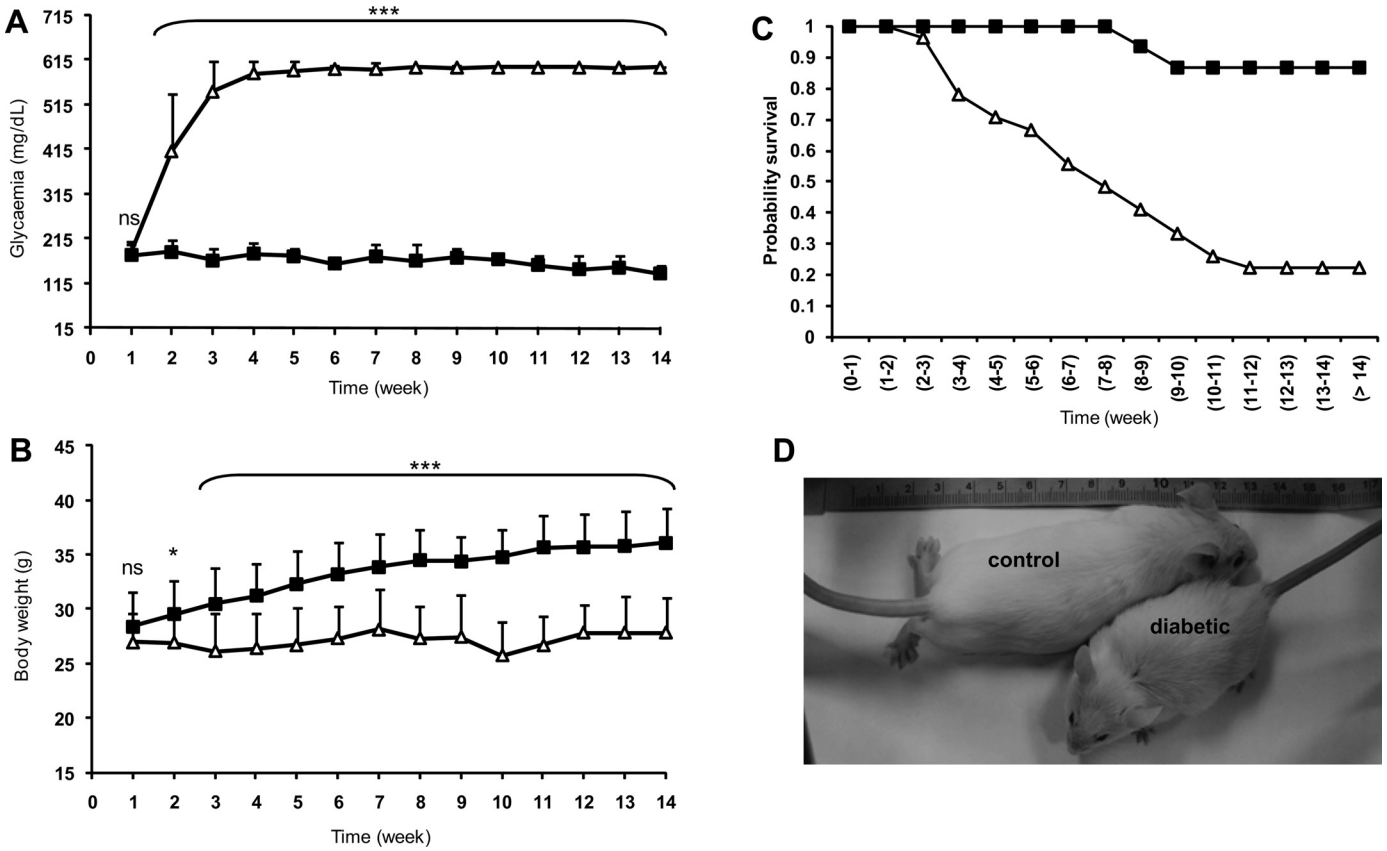

Fig. 1. *A–C*: characterization (glycemia level, body weight, and survival rate) of streptozotocin (STZ)-induced diabetic (△) and control (■) mice. Values are means ± SD of 12 animals per group. *D*: representative image of a 4.5-mo-old control mouse and a 4.5-mo-old STZ-injected diabetic mouse. $*P < 0.05$, $***P < 0.0001$; ns, not significant.

3.2 ± 1.5 μm (n = 40) for diabetic cardiomyocytes (no significant difference, by Student's t-test). Figure 4, *D* and *E*, shows an example of an AFM image from a control isolated cardiomyocyte, and Fig. 4, *G* and *H*, shows an AFM image from a diabetic isolated cardiomyocyte. These images were obtained by scanning a 40 × 40-μm sample area and were used to measure fixed isolated cardiomyocyte height. Height measurements of isolated control and diabetic cardiomyocytes are shown in Fig. 4, *F* and *I*, respectively.

AEM of isolated cardiomyocytes. Figure 5*A* shows force curves from control and diabetic cardiomyocytes. The force curves on live cells showed lower indentation depth in the diabetic than control cardiomyocytes at an equally applied force. A priori, these results indicate that diabetic cardiomyocytes are stiffer. To confirm this, each curve was fitted by a second-order polynomial. To avoid the effect of the substrate on the stiffness measurements, only the first 100 nm of each curve were considered for the polynomial fit. The correlation coefficient (r^2) was >0.98, in each case indicating good agreement between the theoretical model and the experiment. The values obtained for E and γ_a were as follows: E_d = 75.3 kPa and $\gamma_a^d = 2.39 \times 10^{-4}$ J/m^2 for diabetic cardiomyocytes and E_c = 37.4 kPa and $\gamma_a^c = 0.18 \times 10^{-4}$ J/m^2 for control cardiomyocytes.

Figure 5*B* shows the Young's modulus normalized histogram obtained from all diabetic (3 animals, 14 cells, 1,800 force curves) and control (4 animals, 14 cells, and 2,780 force curves) samples. Each histogram was fitted with a Gaussian curve to obtain the mean and standard deviation of the Young's modulus. The AEM of diabetic cardiomyocytes (E_d = 91 ± 14 kPa) was significantly different ($P < 0.01$) from that of control cardiomyocytes (E_c = 43 ± 7 kPa). The mean of the elastic modulus was 112% higher for diabetic than control cardiomyocytes. Figure 5*C* shows the normalized histogram for the work of adhesive force obtained from all samples of each type of cell. Again, a Gaussian fit was used to retrieve the mean value and the standard deviation. For diabetic and control cells, $\gamma_a^d = 2.2 \pm 0.8 \times 10^{-4}$ J/m^2 and $\gamma_a^c = 0.21 \pm 0.04 \times 10^{-4}$ J/m^2, respectively.

AEM of isolated cardiomyocytes in TyBS with different ionic compositions. The AEM of control and diabetic isolated cardiomyocytes was measured in the presence of TyBS containing 100 nM free extracellular Ca^{2+} (low extracellular Ca^{2+} condition; Table 1). Under this experimental condition, the AEM of diabetic cardiomyocytes (E_d = 103 ± 12 kPa) was significantly different ($P < 0.01$) from that of control cardiomyocytes (E_c = 39 ± 6 kPa). However, no significant differences were detected when the AEM of control (E_c = 39 ± 6 kPa) or diabetic (E_d = 103 ± 12 kPa) cardiomyocytes measured with low extracellular Ca^{2+} were compared with the AEM of control (E_c = 41 ± 6 kPa) or diabetic (E_d = 95 ± 14 kPa) cardiomyocytes measured in normal physiological TyBS (containing 1.8 mM extracellular $CaCl_2$; Table 1).

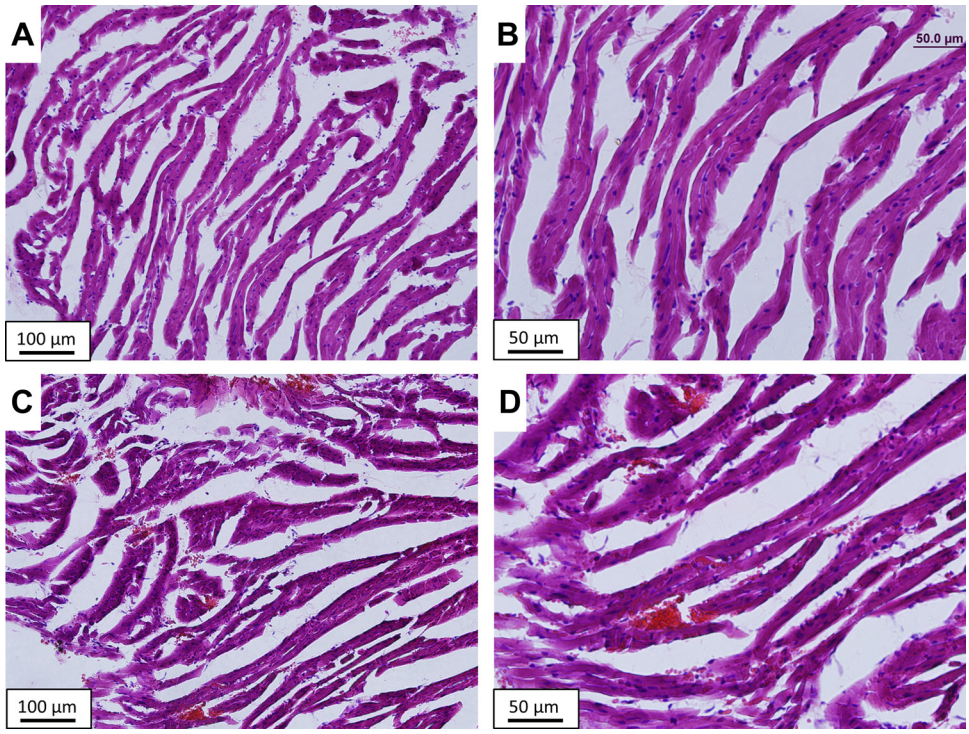

Fig. 2. Myocardial collagen accumulation in heart tissue sections from control and diabetic mice. Representative micrographs show myocardial collagen accumulation in left ventricular (LV) sections from a control mouse (*A* and *B*) and a mouse in which diabetes was induced by STZ injection (*C* and *D*). Cardiac tissues were fixed in 3% paraformaldehyde, cryoprotected in 30% sucrose for 48 h, and embedded in tissue-freezing medium. Sections (5 μm) were stained with hematoxylin and eosin for light-microscopic morphological study. *A* and *B*: LV sections from a control mouse at ×20 and ×40 magnification, respectively. *C* and *D*: LV sections from a STZ-treated mouse at ×20 and ×40 magnification, respectively.

The AEM changed dramatically (in control and diabetic cardiomyocytes) when high K^+ (140 mM) was included in TyBS containing 1.8 mM Ca^{2+} (contraction condition). In control cardiomyocytes, AEM was 106 ± 5 kPa. In diabetic cardiomyocytes, AEM was 324 ± 11 kPa, which was significantly higher than AEM in control cardiomyocytes (Table 1).

F-actin and confocal microscopy. Isolated cardiomyocytes of both groups were obtained and stained with fluorescent phalloidin (see MATERIALS AND METHODS). Control cardiomyocytes showed regular and well-defined actin organization, while diabetic cardiomyocytes showed a more diffuse and irregular actin disposition (Fig. 6). The differences can be visualized in the surface plot of representative control and diabetic cardiomyocytes (Fig. 6, *C* and *F*, respectively). Laser confocal images from 5-μm sections of myocardium stained with fluorescent phalloidin showed well-defined and well-ordered actin filaments in the control samples and disordered and broken actin filaments in the diabetic samples (data not shown).

DISCUSSION

Novel experimental data are presented in this study, which uses the AFM nanoindentation function to analyze, with a nanoscale resolution, isolated cardiomyocytes from control and diabetic mouse hearts. The results suggest that living diabetic cardiomyocytes are stiffer than control cardiomyocytes. Diabetes was induced in mice by STZ administration, which is a well-characterized animal model for induction of type 1 diabetes (5, 24, 31). All diabetic animals showed high blood glucose levels and developed severe symptoms of diabetes, characterized by polyuria, polydipsia, and poor body weight gain (Fig. 1). Previous studies of STZ-induced type 1 diabetic animals showed many functional and structural cardiac muscle

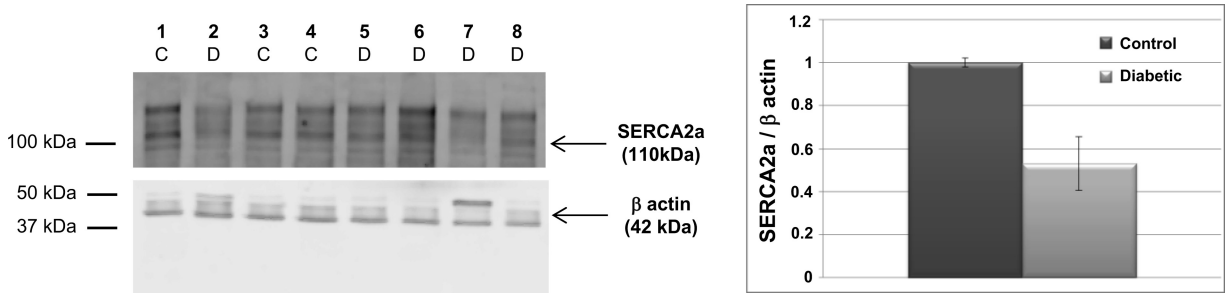

Fig. 3. Inhibition of the sarco/endoplasmic reticulum Ca^{2+}-APTase (SERCA2a) pump. *Left*: representative images obtained from Western blot analysis of LV samples from control and diabetic (STZ-treated) mice. Frozen heart tissue was homogenized in lysis buffer, and proteins were resolved by 10% SDS-PAGE, transferred to a polyvinylidene difluoride membrane, and identified using appropriate antibodies (see MATERIALS AND METHODS). Original captured image of the polyvinylidene difluoride membrane, which was spliced between 50- and 75-kDa protein standards, is shown. *Top blot*: anti-SERCA2a antibody; *bottom blot*: anti-β-actin antibody. *Lanes 1–8* are shown for control (C) and diabetic (D) samples. *Right*: protein bands analyzed using ImageJ software. Significant differences were detected between control ($n = 3$) and diabetic ($n = 5$) bands corresponding to SERCA2a ($P < 0.05$, by Student's *t*-test).

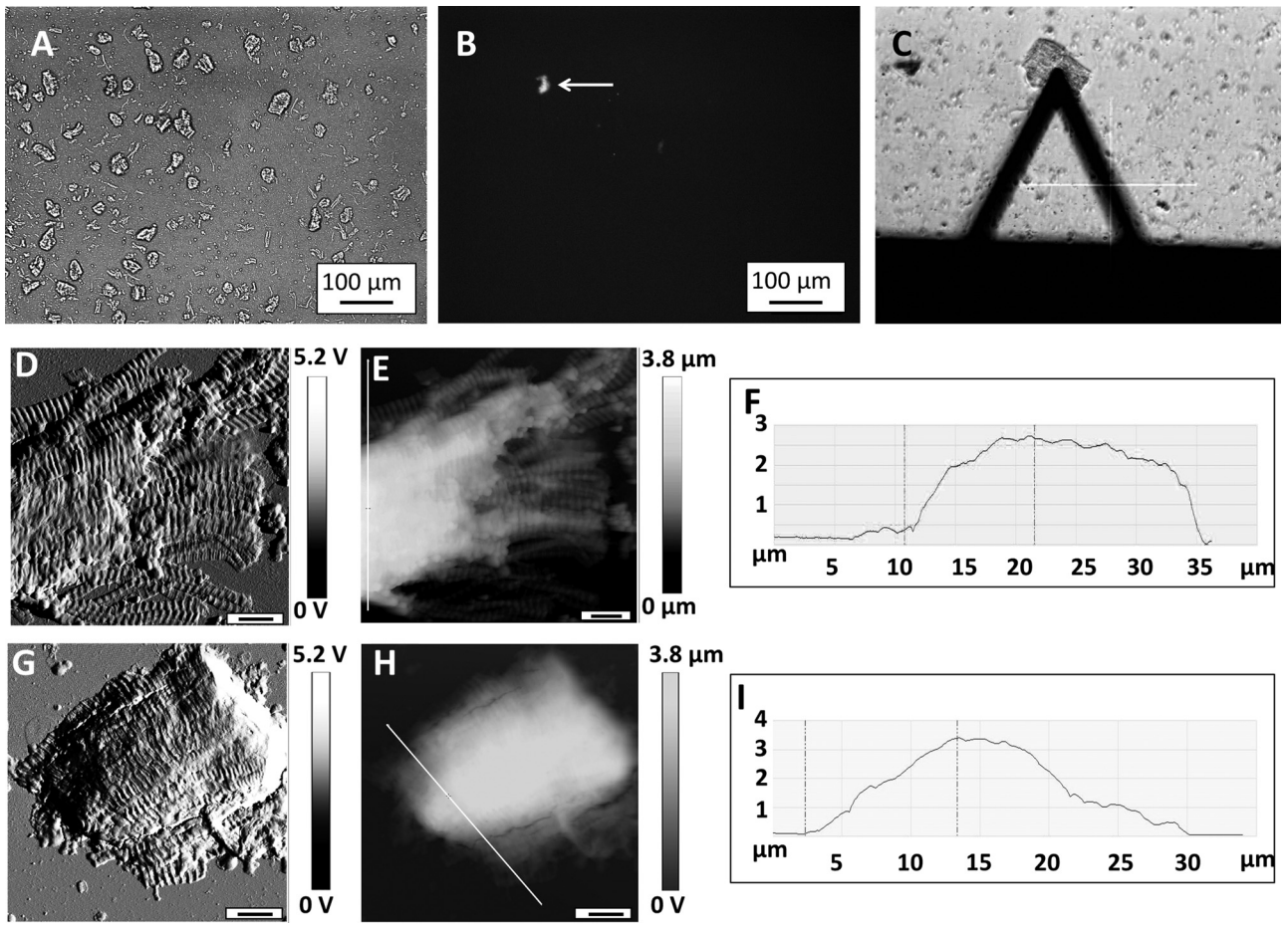

Fig. 4. Optical and atomic force microscopy (AFM) images of isolated cardiomyocytes. *A*: optical microscopy image (×10) of live isolated cardiomyocytes. Cardiomyocytes were isolated (see MATERIALS AND METHODS), incubated for 5 min with propidium iodide, plated on polylysine-treated glass, and imaged using an inverted microscope coupled to the AFM. *B*: fluorescence image (×10) of the preparation shown in *A*. *C*: image (×20) of an isolated cardiomyocyte with the triangle cantilever used to measure force curves. *D*: representative deflection AFM image of a fixed isolated control cardiomyocyte. *E*: control height image. *F*: height measurement of a control cardiomyocyte. *G*: representative deflection AFM image of a fixed isolated diabetic cardiomyocyte. *H*: diabetic height image. *I*: height measurement of a diabetic cardiomyocyte. Scale bars (*D, E, G*, and *H*) = 5 μm.

alterations (5, 19, 24, 30, 31). Consistent with these findings, interstitial collagen accumulation was observed (30) and SERCA2a pump expression was reduced (29–31) in heart tissue sections from diabetic mice (Fig. 2, *C* and *D*, and Fig. 3, respectively). In rats, after a prolonged period of diabetes, a disruption of heart tissue contractile apparatus was reported (19). Control isolated cardiomyocytes stained with phalloidin showed regular and well-defined actin organization, while the diabetic cardiomyocytes showed more diffuse and irregular actin disposition (Fig. 6). Additionally, in sections of diabetic mouse myocardium stained with phalloidin, we detected disordered and broken actin filaments (data not shown). Consistent with these findings, fragmentation of myocardiac fibers in diabetic mice was observed (Fig. 2). Thus, hearts of diabetic animals used in the present study were affected by the induced pathology.

AFM has been employed to measure the viscoelastic response of different cell types (13). The effect of aging and obesity on vascular smooth muscle cell stiffness (8, 21, 38) and the effect of aging on cardiomyocyte stiffness (15) were analyzed using AFM. Cell thickness is an important factor in determining AEM. Substrate contributions to the elastic modulus measurement can be neglected if the AFM tip never indents >10% of the cell thickness (13). AFM images of isolated cardiomyocytes in the present study showed that the height of the smallest cardiomyocyte was 2.5 ± 1.4 μm for the control preparation and 3.2 ± 1.5 μm for the diabetic preparation whereas data were analyzed with a 0.1-μm indentation (Fig. 4). Thus, substrate contribution can be neglected. AFM images were obtained by scanning a 40 × 40-μm sample area with a resolution of 640 × 640 pixels. At this resolution level, images showed no differences between fixed control and diabetic cardiomyocytes. Further AFM image analysis at a higher resolution would be necessary to compare possible changes in diabetic cardiomyocyte topography. It has been reported that cardiomyocytes are softer in the nuclear region and become stiffer toward the periphery (25). To avoid this kind of data interference, all force curves were taken from the middle of the longitudinal axis of all cardiomyocytes from control and diabetic mice.

The AFM technique has been well documented in its ability to measure cytoskeletal components (34). In the case of live isolated cardiomyocytes, AFM indentation measurements register changes in the myocyte sarcolemma, sarcomeric skeleton,

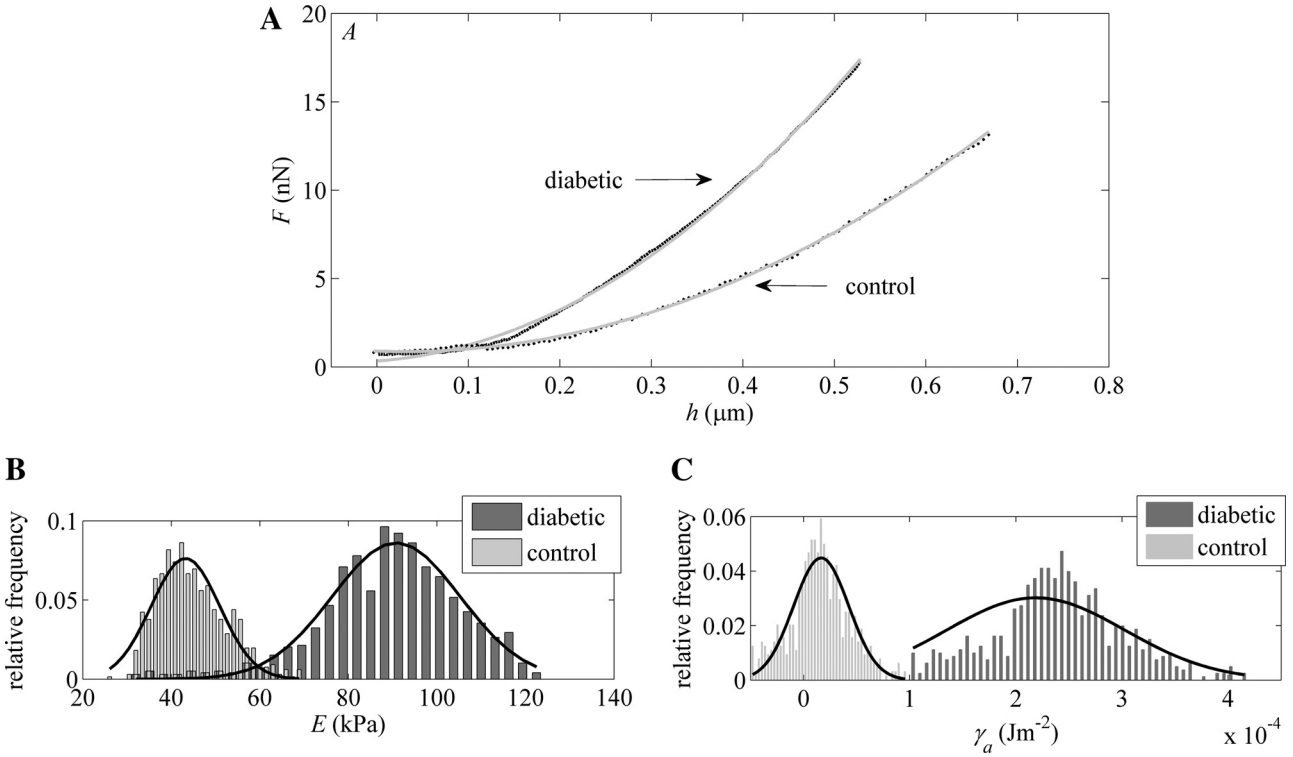

Fig. 5. Force curves, apparent elastic modulus (AEM), and work of adhesive force (γ_a) of isolated cardiomyocytes. *A*: representative force (F) curves of diabetic (dashed line) and control (dotted line) cardiomyocytes. A 2nd-order polynomial fit (continuous line) is also shown for each curve. Correlation coefficient of the fit was >0.98 for each case, indicating the goodness of fit of the model expressed in *Eq. 1*. *h*, Height. *B*: AEM histograms for diabetic and control cardiomyocytes. Sets of data were obtained for 3 diabetic animals (14 cells, 1,800 force curves) and 4 control animals (14 cells, 2,780 force curves). A Gaussian fit was plotted for each histogram to compute the mean and standard deviation of the elastic modulus (*E*). *C*: histograms showing γ_a for diabetic and control cardiomyocytes (data sets are the same as those used in *B*).

and cytoskeletal proteins, such as tubulin, desmin, and actin. In a previous report, the effect of aging in cardiomyocytes of young and old male rats was studied by AFM nanoindentation (15). A significant increase was observed in the AEM of cardiomyocytes from older animals (42.5 ± 1.0 kPa) compared with those from young rats (35.1 ± 0.7 kPa). According to our data, the mean AEM was 112% higher for diabetic than control cardiomyocytes: 91 ± 14 vs. 43 ± 7 kPa in the normal physiological condition (Fig. 5). Therefore, the material properties of cardiomyocytes are affected in a similar manner by diabetes and aging, since both conditions resulted in stiffer cells. However, changes promoted by diabetes seem to be greater than changes promoted by aging.

Table 1. *Apparent elastic modulus of control and diabetic isolated cardiomyocytes in Tyrode buffer solution with different ionic compositions*

	Apparent Elastic Modulus,kPa	
	Control	Diabetic
Normal physiological condition	41 ± 6[a]	95 ± 14[b]
Low extracellular Ca^{2+} condition	39 ± 6[c]	103 ± 12[d]
Contraction condition	106 ± 5[e]	324 ± 11[f]

Values are means ± SD; 800-1,200 force curves were obtained from 4–6 cells from 3 mice. Cardiomyocytes isolated from control and diabetic mice were plated on polylysine-coated glass microslide chambers. Attached cardiomyocytes were incubated in Tyrode buffer solution with different ionic compositions: normal physiological condition (1.8 mM Ca^{2+} and 5.4 mM KCl), low extracellular Ca^{2+} condition (100 nM free Ca^{2+} and 5.4 mM KCl), or contraction condition (1.8 mM Ca^{2+} and 140 mM KCl). Normalized Young's modulus histograms were obtained from all experimental conditions. Each histogram was fitted with a Gaussian curve. Statistical significance is as follows: $P < 0.05$ (by Student's *t*-test) for a vs. b, c vs. d, e vs. f, a or c vs. e, and b or d vs. f; no significant difference for a vs. c and b vs. d.

The AEM of cardiomyocytes isolated from control and diabetic mice was also measured in the presence of TyBS containing 100 nM free extracellular Ca^{2+} (low extracellular Ca^{2+} condition; Table 1). Under this experimental condition, the AEM of diabetic cardiomyocytes (E_d = 103 ± 12 kPa) was significantly different ($P < 0.01$) from that of control cardiomyocytes (E_c = 39 ± 6 kPa). We did not measure cytosolic Ca^{2+} concentration, but in the low extracellular Ca^{2+} condition, in nonstimulated viable cardiomyocytes (absence of PI signal), almost certainly, cytosolic Ca^{2+} concentration will be in the same nanomolar range. Thus it seems reasonable to consider that these cardiomyocytes were at rest. On the other hand, some reports showed no difference between basal Ca^{2+} concentration of control and diabetic cardiomyocytes (20). Therefore, very likely, the difference in the AEM between diabetic and control cardiomyocytes is not related to the contractile state in those conditions but, rather, to changes promoted by diabetes in the material properties of cardiomyocytes. In fact, we observed changes in F-actin organization when isolated control and diabetic cardiomyocytes stained with phalloidin were compared. Control isolated cardiomyocytes showed regular and well-defined actin organization, while the diabetic cardiomyocytes showed more diffuse and irregular

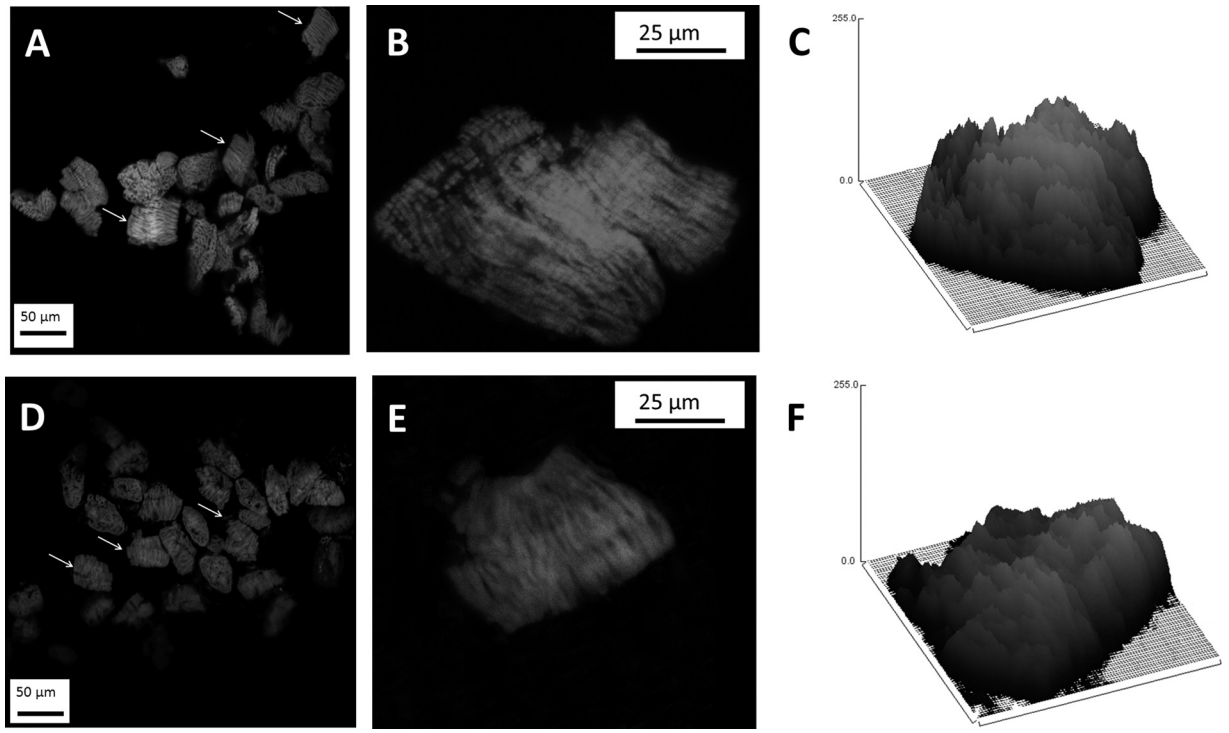

Fig. 6. F-actin in isolated control and diabetic cardiomyocytes. Confocal microscopy images (×40 and ×100) show isolated control and diabetic cardiomyocytes stained with fluorescent phalloidin. Cardiomyocytes were isolated and fixed (see MATERIALS AND METHODS), incubated for 40 min with fluorescent phalloidin, and imaged using a confocal microscope. *A*: control cardiomyocytes (×40). Arrows indicate the most representative control cells, showing regular and well-defined actin organization. *B*: control cardiomyocyte (×100). *C*: surface plot of cell image in *B*. *D*: diabetic cardiomyocytes (×40). Arrows indicate the most representative diabetic cells showing more diffuse and irregular actin disposition. *E*: diabetic cardiomyocyte (×100). *F*: surface plot of cell image in *E*.

actin disposition (Fig. 6). On the other hand, no significant differences were found between the AEM of control or diabetic cardiomyocytes measured in the low extracellular Ca^{2+} condition and the normal physiological condition (Table 1). A possible explanation for the absence of differences is that viable cardiomyocytes were selected for all AFM measurements. Very likely, their cytosolic Ca^{2+} concentration was in the nanomolar range (resting). The AEM changed dramatically (in control and diabetic cardiomyocytes) when high (140 mM) K^+ was included in TyBS containing 1.8 mM Ca^{2+} (contraction condition). In control cardiomyocytes, AEM was 106 ± 5 kPa. On the other hand, AEM was significantly higher in diabetic than control cardiomyocytes and was 324 ± 11 kPa. The dramatic change in AEM in control and diabetic cardiomyocytes measured in high-K^+ TyBS might be explained by the opening of membrane Ca^{2+} channels, the increase in cytosolic Ca^{2+} concentration, and cardiomyocyte contraction (contraction condition). Even in this condition, the AEM was significantly higher in diabetic than control cardiomyocytes. Thus the difference between diabetic and control cardiomyocytes holds up in this altered contractile state, and we believe this is, in part, due to the cytoskeletal state in diabetic cardiomyocytes. Therefore, diabetic cardiomyocytes were stiffer than control cardiomyocytes in all tested conditions, supporting the idea that the mechanical properties of live cardiomyocytes were affected by diabetes.

It has been reported that excessive fibrosis, deposition of advanced glycation end products, and cardiomyocyte stiffness are mechanisms responsible for raising myocardial stiffness in diabetes mellitus (4, 10, 32). Cardiomyocyte stiffness was determined by measuring resting tension (passive force at the same sarcomere length, using a force transducer and a piezoelectric motor) in single isolated cardiomyocytes. According to previously mentioned reports, resting tension was measured in frozen biopsy samples that, prior to experiments, were defrosted, mechanically disrupted, and incubated with Triton X-100. This procedure provokes disruption of sarcolemmal and sarcoplasmic membranes. Therefore, isolated cardiomyocytes became dependent on externally supplied Ca^{2+} for active force development. Thus the elevation of passive force was attributed to alterations of myofilament or cytoskeletal proteins. Hypophosphorylation of the cytoskeletal protein titin stiff isoform was suggested to be responsible for the elevation of passive force in diabetic cardiomyocytes (10).

According to our data, the mean AEM was higher (stiffer) for diabetic than control cardiomyocytes (Fig. 5*D*). Thus our results are in agreement with the previously mentioned studies of isolated cardiomyocytes with disrupted membranes. Since we checked the viability of the isolated cardiomyocytes before and after force curve measurements (by checking the absence of PI fluorescence using the inverted microscope coupled to the AFM), we can extend the observation to live cardiomyocytes. In our studies, cardiomyocyte membranes were undisrupted, suggesting that changes in membranes of diabetic cardiomyocytes probably contribute to the higher elastic modulus measured by AFM nanoindentation. Additionally, changes in F-actin in isolated cardiomyocytes of diabetic mice (confocal images) indicate changes in their actin organization, which is probably responsible for the higher elastic modulus of the diabetic cardiomyocytes.

As shown in Fig. 5*C*, adhesive force was higher in diabetic than control cardiomyocytes. Adhesive force represents the interaction force between the tip and the sample. Most probably, as cardiomyocytes' sarcolemmas were undisrupted, the contribution of the sarcolemma to adhesive force is an important component. Adhesive force changed from $\gamma_a^c = 0.21 \pm 0.04 \times 10^{-4}$ J/m^2 in control cardiomyocytes to $\gamma_a^d = 2.2 \pm 0.8 \times 10^{-4}$ J/m^2 in diabetic cardiomyocytes. This 10.5-fold change in γ_a suggests that cardiomyocytes' sarcolemmas were deeply affected by diabetes. In the present study we showed that adhesive force is greater in diabetic than control cardiomyocytes. These results suggest a change (i.e., an increase) in the number and/or the activation state of adhesion molecules on the surface of the diabetic cardiomyocytes. Further studies are needed to understand the physiological meaning of these results.

In summary, our data show that 3 mo of type 1 diabetes provokes changes in myocardial fibers of mouse hearts (fragmentation and disordering), interstitial collagen deposition, reduction of the SERCA2a pump expression, and changes in F-actin organization. Moreover, the data show that live isolated diabetic cardiomyocytes are stiffer than control cardiomyocytes in all tested conditions, suggesting that the material properties of live cardiomyocytes change with diabetes. Hence, it is very likely that a change in the material properties is an important factor in raising myocardial stiffness in vivo. Further studies are necessary to identify the molecules that are responsible for the increment in stiffness of live diabetic cardiomyocytes. Our data strongly suggest that actin is one of these molecules.

It will be interesting to extend the observations in the present study, in which a type 1 diabetes model was used, to a type 2 diabetes animal model.

ACKNOWLEDGMENTS

We thank Maria Bausero for critically reviewing the manuscript and Rita Pessano for the English language revision of the manuscript.

GRANTS

This research was supported by the Agencia Nacional de Investigación e Innovación, Uruguay (ANII, FCE_2009_1_2887) and partially by PEDECIBA, Uruguay.

DISCLOSURES

No conflicts of interest, financial or otherwise, are declared by the authors.

AUTHOR CONTRIBUTIONS

J.C.B. is responsible for conception and design of the research; J.C.B., N.B., A.I.Z., I.R., V.B., N.O., and J.P.D. performed the experiments; J.C.B., N.B., A.I.Z., I.R., V.B., N.O., and J.P.D. analyzed the data; J.C.B., N.B., A.I.Z., I.R., V.B., N.O., and J.P.D. interpreted the results of the experiments; J.C.B., N.B., A.I.Z., I.R., V.B., N.O., and J.P.D. prepared the figures; J.C.B., N.B., A.I.Z., and J.P.D. drafted the manuscript; J.C.B. and N.B. edited and revised the manuscript; J.C.B. approved the final version of the manuscript.

REFERENCES

1. **Aksoy P, Escande C, White TA, Thompson M, Soares S, Benech JC, Chini EN.** Regulation of SIRT 1 mediated NAD dependent deacetylation: a novel role for the multifunctional enzyme CD38. *Biochem Biophys Res Commun* 349: 353–359, 2006.
2. **Benech JC, Wolosker H, de Meis L.** Reversal of the Ca^{2+} pump of blood platelets. *Biochem J* 306: 35–38, 1995.
3. **Berg TJ, Snorgaard O, Faber J, Torjesen PA, Hildebrandt P, Mehlsen J, Hanssen KF.** Serum levels of advanced glycation end products are associated with left ventricular diastolic function in patients with type 1 diabetes. *Diabetes Care* 22: 1186–1190, 1999.
4. **Borbely A, van der Velden J, Papp Z, Bronzwaer JG, Edes I, Stienen GJ, Paulus WJ.** Cardiomyocyte stiffness in diastolic heart failure. *Circulation* 111: 774–781, 2005.
5. **Boudina S, Abel ED.** Diabetic cardiomyopathy revisited. *Circulation* 115: 3213–3223, 2007.
6. **Brum G, Flockerzi V, Hofmann F, Osterrieder W, Trautwein W.** Injection of catalytic subunit of cAMP-dependent protein kinase into isolated cardiac myocytes. *Pflügers Arch* 398: 147–154, 1983.
7. **Collinsworth AM, Zhang S, Kraus WE, Truskey GA.** Apparent elastic modulus and hysteresis of skeletal muscle cells throughout differentiation. *Am J Physiol Cell Physiol* 283: C1219–C1227, 2002.
8. **Chen JY, Tsai PJ, Tai HC, Tsai RL, Chang YT, Wang MC, Chiou YW, Yeh ML, Tang MJ, Lam CF, Shiesh SC, Li YH, Tsai WC, Chou CH, Lin LJ, Wu HL, Tsai YS.** Increased aortic stiffness and attenuated lysyl oxidase activity in obesity. *Arterioscler Thromb Vasc Biol* 33: 839–846, 2013.
9. **Fabiato A, Fabiato F.** Calculator programs for computing the composition of the solutions containing multiple metals and ligands used for experiments in skinned muscle cells. *J Physiol (Paris)* 75: 463–505, 1979.
10. **Falcão-Pires I, Hamdani N, Borbély A, Gavina C, Schalkwijk CG, van der Velden J, van Heerebeek L, Stienen GJ, Niessen H, Leite-Moreira AF, Paulus WJ.** Diabetes mellitus worsens diastolic left ventricular dysfunction in aortic stenosis through altered myocardial structure and cardiomyocyte stiffness. *Circulation* 124: 1151–1159, 2011.
11. **Garcia MJ, McNamara PM, Gordon T, Kannel WB.** Morbidity and mortality in diabetics in the Framingham population. Sixteen year follow-up study. *Diabetes* 23: 105–111, 1974.
12. **Kannel WB, McGee DL.** Diabetes and cardiovascular disease. The Framingham Study. *JAMA* 241: 2035–2038, 1979.
13. **Kuznetsova TG, Starodubtseva MN, Yegorenkov NI, Chizhik SA, Zhdanov RI.** Atomic force microscopy probing of cell elasticity. *Micron* 38: 824–833, 2007.
14. **Li QS, Lee GY, Ong CN, Lim CT.** AFM indentation study of breast cancer cells. *Biochem Biophys Res Commun* 374: 609–613, 2008.
15. **Lieber SC, Aubry N, Pain J, Diaz G, Kim SJ, Vatner SF.** Aging increases stiffness of cardiac myocytes measured by atomic force microscopy nanoindentation. *Am J Physiol Heart Circ Physiol* 287: H645–H651, 2004.
16. **Mathur AB, Collinsworth AM, Reichert WM, Kraus WE, Truskey GA.** Endothelial, cardiac muscle and skeletal muscle exhibit different viscous and elastic properties as determined by atomic force microscopy. *J Biomech* 34: 1545–1553, 2001.

16a. **Meininger GA.** *The central importance of the cytoskeleton for increased cell stiffness in cardiovascular disease*. Focus on "Diabetes increases stiffness of live cardiomyocytes measured by atomic force microscopy nanoindentation." *Am J Physiol Cell Physiol* (August 13, 2014). doi: 10.1152/ajpcell.00279.2014.

17. **Muller DJ, Dufrene YF.** Atomic force microscopy: a nanoscopic window on the cell surface. *Trends Cell Biol* 21: 461–469, 2011.
18. **Murcia AM, Hennekens CH, Lamas GA, Jimenez-Navarro M, Rouleau JL, Flaker GC, Goldman S, Skali H, Braunwald E, Pfeffer MA.** Impact of diabetes on mortality in patients with myocardial infarction and left ventricular dysfunction. *Arch Intern Med* 164: 2273–2279, 2004.
19. **Nemoto O, Kawaguchi M, Yaoita H, Miyake K, Maehara K, Maruyama Y.** Left ventricular dysfunction and remodeling in streptozotocin-induced diabetic rats. *Circ J* 70: 327–334, 2006.
20. **Pierce GN, Russell JC.** Regulation of intracellular Ca^{2+} in the heart during diabetes. *Cardiovasc Res* 34: 41–47, 1997.
21. **Qiu H, Zhu Y, Sun Z, Trzeciakowski JP, Gansner M, Depre C, Resuello RR, Natividad FF, Hunter WC, Genin GM, Elson EL, Vatner DE, Meininger GA, Vatner SF.** Vascular smooth muscle cell stiffness as a mechanism for increased aortic stiffness with aging. *Circ Res* 107: 615–619, 2010.
22. **Radmacher M, Fritz M, Kacher CM, Cleveland JP, Hansma PK.** Measuring the viscoelastic properties of human platelets with the atomic force microscope. *Biophys J* 70: 556–567, 1996.
23. **Shah AM, Uno H, Kober L, Velazquez EJ, Maggioni AP, MacDonald MR, Petrie MC, McMurray JJ, Califf RM, Pfeffer MA, Solomon SD.** The inter-relationship of diabetes and left ventricular systolic function on outcome after high-risk myocardial infarction. *Eur J Heart Fail* 12: 1229–1237, 2010.

24. **Shiomi T, Tsutsui H, Ikeuchi M, Matsusaka H, Hayashidani S, Suematsu N, Wen J, Kubota T, Takeshita A.** Streptozotocin-induced hyperglycemia exacerbates left ventricular remodeling and failure after experimental myocardial infarction. *J Am Coll Cardiol* 42: 165–172, 2003.
25. **Shroff SG, Saner DR, Lal R.** Dynamic micromechanical properties of cultured rat atrial myocytes measured by atomic force microscopy. *Am J Physiol Cell Physiol* 269: C286–C292, 1995.
26. **Sirghi L, Ponti J, Broggi F, Rossi F.** Probing elasticity and adhesion of live cells by atomic force microscopy indentation. *Eur Biophys J* 37: 935–945, 2008.
27. **Solomon SD, St. John Sutton M, Lamas GA, Plappert T, Rouleau JL, Skali H, Moye L, Braunwald E, Pfeffer MA.** Ventricular remodeling does not accompany the development of heart failure in diabetic patients after myocardial infarction. *Circulation* 106: 1251–1255, 2002.
28. **Stone PH, Muller JE, Hartwell T, York BJ, Rutherford JD, Parker CB, Turi ZG, Strauss HW, Willerson JT, Robertson T, et al.** The effect of diabetes mellitus on prognosis and serial left ventricular function after acute myocardial infarction: contribution of both coronary disease and diastolic left ventricular dysfunction to the adverse prognosis. The MILIS Study Group. *J Am Coll Cardiol* 14: 49–57, 1989.
29. **Suarez J, Scott B, Dillmann WH.** Conditional increase in SERCA2a protein is able to reverse contractile dysfunction and abnormal calcium flux in established diabetic cardiomyopathy. *Am J Physiol Regul Integr Comp Physiol* 295: R1439–R1445, 2008.
30. **Sulaiman M, Matta MJ, Sunderesan NR, Gupta MP, Periasamy M, Gupta M.** Resveratrol, an activator of SIRT1, upregulates sarcoplasmic calcium ATPase and improves cardiac function in diabetic cardiomyopathy. *Am J Physiol Heart Circ Physiol* 298: H833–H843, 2010.
31. **Trost SU, Belke DD, Bluhm WF, Meyer M, Swanson E, Dillmann WH.** Overexpression of the sarcoplasmic reticulum Ca^{2+}-ATPase improves myocardial contractility in diabetic cardiomyopathy. *Diabetes* 51: 1166–1171, 2002.
32. **van Heerebeek L, Hamdani N, Handoko ML, Falcao-Pires I, Musters RJ, Kupreishvili K, Ijsselmuiden AJ, Schalkwijk CG, Bronzwaer JG, Diamant M, Borbely A, van der Velden J, Stienen GJ, Laarman GJ, Niessen HW, Paulus WJ.** Diastolic stiffness of the failing diabetic heart: importance of fibrosis, advanced glycation end products, and myocyte resting tension. *Circulation* 117: 43–51, 2008.
33. **Van Hoeven K, Factor S.** A comparison of the pathological spectrum of hypertensive, diabetic, and hypertensive-diabetic heart disease. *Circulation* 82: 848–855, 1990.
34. **Vinckier A, Semenza G.** Measuring elasticity of biological materials by atomic force microscopy. *FEBS Lett* 430: 12–16, 1998.
35. **Wild S, Roglic G, Green A, Sicree R, King H.** Global prevalence of diabetes: estimates for the year 2000 and projections for 2030. *Diabetes Care* 27: 1047–1053, 2004.
36. **Wright JR, Jr., Mendola J, and Lacy PE.** Effect of niacin/nicotinamide deficiency on the diabetogenic effect of streptozotocin. *Experientia* 44: 38–40, 1988.
37. **Wu X, Sun Z, Foskett A, Trzeciakowski JP, Meininger GA, Muthuchamy M.** Cardiomyocyte contractile status is associated with differences in fibronectin and integrin interactions. *Am J Physiol Heart Circ Physiol* 298: H2071–H2081, 2010.
38. **Zhu Y, Qiu H, Trzeciakowski JP, Sun Z, Li Z, Hong Z, Hill MA, Hunter WC, Vatner DE, Vatner SF, Meininger GA.** Temporal analysis of vascular smooth muscle cell elasticity and adhesion reveals oscillation waveforms that differ with aging. *Aging Cell* 11: 741–750, 2012.